THE NEUTRAL ENVELOPES AROUND AGB AND POST-AGB OBJECTS

Circumstellar Molecules

H. OLOFSSON
Stockholm Observatory
S-133 36 Saltsjöbaden, Sweden

Abstract. The circumstellar gas/dust envelopes of stars on and beyond the asymptotic giant branch harbor an impressive number of different molecular species and their isotopic variants. Some of these molecules are of photospheric origin, but the majority have been produced through various chemical processes in the envelope. This chemistry depends primarily on the chemical composition of the gas (i.e., C/O<1 or >1), but the conditions also change as the central star evolves. In this review we present circumstellar molecular abundance and isotope ratio estimates, and discuss how they can be used in the study of the late evolution of stars, which in extreme cases may become heavily obscured.

1. Introduction

The circumstellar envelopes (CSEs) around asymptotic giant branch (AGB) stars, formed by intense stellar mass loss, have proven efficient not only in protecting the molecules that participate in the gas outflow from the star, but also to provide the necessary conditions for the production of new molecules by a circumstellar chemistry. This chemistry is to a large extent different from the interstellar chemistry, mainly due to the introduction of a new (and short) time scale, the expansion time scale of the CSE, and the lesser importance of ion–molecule reactions. Also, the CSEs come in two, for the chemistry very important, distinct classes of elemental composition, C/O<1 and C/O>1 (in fact, also the C≈O variant exists).

The relative simplicity of a CSE — i.e., its (at least on the AGB) largely spherical geometry, a density distribution determined by the stellar mass loss history and the expansion, a kinematics that is dominated by expansion at a constant velocity, and the central star radiation field — makes

E. F. van Dishoeck (ed.), Molecules in Astrophysics: Probes and Processes, 457–468.

it a particularly suitable laboratory for the study of molecular processes. Likewise, the molecules are useful probes of the properties of the circumstellar medium, as well as provide important information on the properties of the central, highly evolved star. The latter is particularly important for the highly obscured objects where normal spectroscopic methods in the infrared and the optical range fail.

2. The physical properties of CSEs

The mass ejection during the AGB appears to have an overall spherical symmetry, with (possibly) a slight density enhancement in the equatorial region. It also appears that as soon as the AGB evolution is terminated, a (probably isotropic) high–velocity wind starts to blow and initially molecular material along the polar axis is accelerated to high velocities. The acceleration gradually affects material at lower latitudes, and as the evolution towards, and during, the planetary nebula (PN) stage proceeds, the CSE eventually takes the form of a thick ring of highly disrupted molecular gas. Olofsson (1994, 1997) has presented reviews on this topic.

The density structure, $\rho(r,\theta,\varphi)$, is determined by the continuity equation, $\dot{M}(t-t_{\rm ret},\theta,\varphi) = 4\pi r^2 \rho v_{\rm e}$ [where $t_{\rm ret}$ is determined by r and $v_{\rm e}(r)$], and for a constant mass loss rate, $\dot{M}$, and expansion velocity, $v_{\rm e}$, the H_2 number density is given by,

$$n_{\rm H_2} = 10^6 \left(\frac{\dot{M}_{\rm H_2}}{10^{-6}\ {\rm M_\odot\,yr^{-1}}}\right)\left(\frac{15\ {\rm km\,s^{-1}}}{v_{\rm e}}\right)\left(\frac{10^{15}\,{\rm cm}}{r}\right)^2\ {\rm cm^{-3}}. \quad (1)$$

Thus, $n_{\rm H_2}$ covers a fairly broad range. However, there is growing evidence that the circumstellar medium has quite a clumpy structure (Guélin et al. 1993; Olofsson et al. 1996; Olofsson 1997). Therefore, results based on the smooth wind approximation may have to be treated with some caution.

The kinetic temperature is determined by the initial conditions, the adiabatic cooling during expansion, and various heating and cooling mechanisms, where the heating due to grain-gas collisions dominate (Truong–Bach et al. 1990). The kinetic temperature law can be approximated by

$$T_{\rm k}(r) = T_0(\dot{M})\left(\frac{10^{15}\,{\rm cm}}{r}\right)^{0.7}, \quad (2)$$

where $T_0(\dot{M})$ depends on the mass loss rate (e.g., Kastner 1992), such that low–$\dot{M}$ CSEs are warmer than high–$\dot{M}$ CSEs [$T_0 \approx 300\,{\rm K}$ at $\dot{M} = 2\times10^{-5}\,{\rm M_\odot\,yr^{-1}}$ (Huggins et al. 1988)]. It should be noted that adiabatic cooling may lead to very low temperatures in high–velocity, high–$\dot{M}$ CSEs.

https://doi.org/10.1017/S007418090000961X Published online by Cambridge University Press

The central radiation field will be that of a cool, luminous red giant during the AGB, a warm, luminous central core on the early post–AGB, and a hot, less luminous compact core (a white dwarf) during the PN evolution. Some red giants also show chromospheric activity (see e.g., Johnson et al. 1995). Finally, the interstellar UV radiation field plays a very important role, since it determines the sizes of the molecular envelopes through photodissociation (Mamon et al. 1988).

As mentioned above the elemental composition of a CSE may be very different from that of the ISM, in particular C/O>1, due to the evolution of the central star.

3. Circumstellar molecules

The era of radio observations of circumstellar molecules started in 1970 when Solomon et al. (1971) detected CO in the IR–bright carbon star IRC+10216. Since then the progress has been almost breathtaking and today we count 49 molecular species detected at radio wavelengths in CSEs around late stellar objects of different evolutionary stages, which are summarized in Table 1. Even though this appears impressive, it should be noted that ≈20 of these species have been detected only in IRC+10216, only ≈7 objects have been detected in more than 10 species, and only in one source (IRC+10216) has a reasonable number (≈ 15) of molecular emissions been mapped in some detail. Reasonable statistics exist only for the maser line emission from OH, H_2O, and SiO, and for the "thermal" emission from CO, and to some extent, HCN.

An additional 8 (non-polar) species have only been detected at infrared wavelengths: H_2, C_3, CO_2, C_2H_2, C_5, CH_4, SiH_4, C_2H_4. At optical wavelengths there are also definite detections of e.g. C_2 and CH^+ (Bakker et al. 1996).

4. Circumstellar molecular abundances

The relatively simple physical structure of a CSE lends the hope that accurate molecular abundances can be estimated. However, this simplicity (in the sense of the boundary conditions) is partly counteracted by the lack of enough observational spatial resolution combined with the rapidly changing physical and chemical conditions with location in the CSE. Furthermore, transition strengths and collisional cross sections are not available for the great majority of the molecules. Therefore, one is in general restricted to a simple analysis which nevertheless should lead to reasonably accurate abundance estimates for those species observed in, at least, a few lines.

TABLE 1. Molecules detected at radio wavelengths in envelopes around AGB and post–AGB objects of different chemistries (O: C/O<1; S: C/O≈1; C: C/O>1). The (rough) number of sources Σ detected in each species is also given.

Molecule	Chemistry			Σ	Molecule	Chemistry			Σ
	O	S	C			O	S	C	
2-atomic:									
AlCl			*	1	NaCl			*	1
AlF			*	1	OH	*			2000
CO	*	*	*	500	SiC			*	2
CN	*	*	*	50	SiN			*	1
CP			*	1	SiO	*	*	*	450
CS	*	*	*	40	SiS	*		*	15
KCl			*	1	SO	*			25
3-atomic:									
C_2H			*	10	MgCN			*	1
C_2S			*	4	MgNC			*	1
HCN	*	*	*	130	NaCN			*	1
H_2O	*			300	OCS	*			1
H_2S	*			20	SiC_2			*	5
HNC	*		*	15	SO_2	*			20
4-atomic:									
ℓ-C_3H			*	2	HC_2N			*	1
C_3N			*	5	H_2CO	*			2
C_3S			*	1	NH_3	*		*	6
5-atomic:									
C_4H			*	6	HC_3N			*	10
C_4Si			*	1	HC_2NC			*	1
c-C_3H_2			*	7	H_2C_3			*	1
6-atomic:									
C_5H			*	1	H_2C_4			*	1
CH_3CN			*	6					
7-atomic:									
C_6H			*	1	HC_5N			*	6
9-atomic:									
C_8H			*	1	HC_7N			*	2
11-atomic:									
HC_9N			*	3					
Mol. ions:									
CO^+			*	1	HCO^+			*	10
NH_2^+			*	2					

https://doi.org/10.1017/S007418090000961X Published online by Cambridge University Press

4.1. COLUMN DENSITY AND THE ROTATION TEMPERATURE DIAGRAM

Using the simplest possible approximations, a spherical CSE formed by a constant mass loss rate, a constant abundance with respect to H_2, $f_X = [X]/[H_2]$, within the radial range R_i to R_e, and a constant excitation temperature T_{ex} that applies to all levels, we calculate that the abundance of species X, estimated from the line $X(u \rightarrow l)$, is given by,

$$f_X = 1.7 \times 10^{-28} I_{X(u\rightarrow l)} \frac{v_e B D}{\dot{M}_{H_2}} \frac{Q(T_{ex})\nu_{ul}^2}{g_u A_{ul}} \frac{e^{E_l/kT_{ex}}}{\int_{x_i}^{x_e} e^{-4\ln 2\, x^2}\, dx} \qquad (3)$$

where $I_{X(u\rightarrow l)}$ is the velocity–integrated intensity given in $K\,km\,s^{-1}$, v_e is in $km\,s^{-1}$, B is the full half power beam width in arc seconds, D is the distance to the source in pc, $\dot{M}_{H_2}$ is in $M_\odot\,yr^{-1}$, Q is the partition function, ν_{ul} is the line frequency in GHz, g_u is the statistical weight of the upper level, A_{ul} is the Einstein A–coefficient, E_l is the energy of the lower level, and $x_{i,e} = R_{i,e}/BD$ (Olofsson et al. 1993).

In the case that a molecular species is observed in a number of lines, the best abundance estimate is obtained using a rotation temperature diagram. This is obtained by rewriting Eq. (3) in the form

$$\ln\left(\frac{(I/\eta)\nu_{ul}^2}{g_u A_{ul}}\right) + \ln\left(1.9 \times 10^3 \frac{Q(T_{ex})}{\bar{N}_{B,X}}\right) = -\frac{E_l}{kT_{ex}} \qquad (4)$$

where $\eta = \int_{x_i}^{x_e} e^{-4\ln 2\, x^2}\, dx$ takes care of the beam filling, and we have introduced a "beam–averaged" column density (given in cm^{-2})

$$\bar{N}_{B,X} = \frac{2(\ln 2) f_X \dot{M}_{H_2}}{\pi m_H v_e B D} \qquad (5)$$

which is, of course, defined only for a single value of B. However, most results on CSEs are not based on this form of the rotation temperature diagram. Instead, the more traditional form, used in the study of the ISM, is adopted, where

$$\eta = \frac{\theta_S^2}{\theta_S^2 + B^2} \quad \text{gaussian source} \qquad (6)$$

$$\eta = 1 - e^{-4\ln 2 (R_e/B)^2} \quad \text{disc source,} \qquad (7)$$

which is actually not the correct beam filling factor (θ_S is the full width at half maximum of the source). The column density in this case rather takes the form of a "source–averaged" column density (note that the analysis is

https://doi.org/10.1017/S007418090000961X Published online by Cambridge University Press

no longer fully stringent). A simple calculation, with the above assumptions on the CSE, results in

$$\bar{N}_{\rm S,X} = \frac{f_{\rm X}\dot{M}_{\rm H_2}}{2\pi m_{\rm H} v_{\rm e}} \frac{R_{\rm e} - R_{\rm i}}{R_{\rm e}^2} \,. \tag{8}$$

A straight line fit to the data–points in the $(\ln[(I/\eta)\nu_{ul}^2/g_u A_{ul}],\ E_l/k)$–diagram results in an estimate of $\bar{N}_{\rm S,X}$ and $T_{\rm ex}$.

In Table 2 all abundance estimates obtained in this way are compiled. They are mainly based on spectral scans and directed searches at various telescopes (e.g., Cernicharo & Guélin 1987, 1996; Guélin et al. 1990; Avery et al. 1992; Groesbeck et al. 1994; Turner et al. 1994; Kawaguchi et al. 1995; Ziurys et al. 1995).

Finally, one should note that absorption line observations result in the estimate of the radial column density,

$$N_{\rm X} = \frac{f_{\rm X}\dot{M}_{\rm H_2}}{8\pi m_{\rm H} v_{\rm e}} \left(\frac{1}{R_{\rm i}} - \frac{1}{R_{\rm e}}\right) \approx \frac{R_{\rm e}}{4R_{\rm i}} \bar{N}_{\rm S,X} \ \ (\text{if } R_{\rm i} \ll R_{\rm e}) \,, \tag{9}$$

which differs significantly from the "source–averaged" column density.

4.2. ABUNDANCE RATIOS

Abundance ratios are expected to be more reliable than absolute abundances, and hence they will put better constraints on the chemical models, in particular when combined with detailed maps of the emissions (e.g., Guélin et al. 1993). We will here concentrate on the results on IRC+10216. Of special interest are the long carbon–chain molecules of various kinds: HCN / HC_3N / HC_5N / HC_7N / HC_9N = 1 / 0.1 / 0.05 / 0.005 / 0.001, C_2H / C_3H / C_4H / C_5H / C_6H / C_8H = 1 / 0.01 / 0.5 / 0.05 / 0.05 / 0.001, CS / C_2S / C_3S = 1 / 0.05 / 0.02, CSi / C_4Si =1 / 0.1. Also the low abundance of related species, e.g., HC_2N / HC_3N = 0.01, HC_2NC / HC_3N = 0.01, CH_3CN / HCN = 0.0003, and CH_3CN / HC_2N = 0.3 are significant. Of further interest are the abundance ratios (MgCN+MgNC) / NaCN = 1 (Mg / Na=17), AlCl / KCl / NaCl = 1 / 0.01 / 0.01 (Al / K / Na = 1 / 21 / 0.6), and AlF / MgF / CaF = 1 / $\leq$0.1 / $\leq$0.3 (Al / Mg / Ca = 1 / 9 / 0.7), which are very different from the elemental abundance ratios (the main isotope ratios are given in the parentheses). This shows that the chemistry has had a significant effect on the abundances.

5. Elemental composition

An ultimate goal would be to estimate the elemental composition of these highly evolved stars, in particular the highly obscured ones, from the circumstellar molecular line emission. In principle, changes in the elemental

https://doi.org/10.1017/S007418090000961X Published online by Cambridge University Press

TABLE 2. Molecular abundances with respect to H_2 in AGB envelopes

Molecule	Chemistry		Molecule	Chemistry	
	O	C		O	C
2-atomic:					
AlCl		2×10^{-7}	NaCl		1×10^{-9}
AlF		4×10^{-8}	OH	2×10^{-5}	
CO	5×10^{-4}	1×10^{-3}	SiC		4×10^{-8}
CN	7×10^{-8}	2×10^{-6}	SiN		2×10^{-8}
CP		2×10^{-8}	SiO	5×10^{-6}	1×10^{-7}
CS	1×10^{-7}	2×10^{-6}	SiS	7×10^{-7}	1×10^{-6}
KCl		2×10^{-9}	SO	2×10^{-6}	
3-atomic:					
C_3		1×10^{-6}	HNC	8×10^{-8}	1×10^{-7}
C_2H		1×10^{-6}	MgCN		1×10^{-9}
C_2S		1×10^{-7}	MgNC		2×10^{-8}
HCN	5×10^{-7}	1×10^{-5}	NaCN		2×10^{-8}
H_2O	3×10^{-4}		SiC_2		3×10^{-7}
H_2S	1×10^{-5}		SO_2	2×10^{-6}	
4-atomic:					
ℓ-C_3H		3×10^{-8}	HC_2N		8×10^{-9}
C_3N		2×10^{-7}	H_2CO	2×10^{-8}	
C_3S		3×10^{-8}	NH_3	4×10^{-6}	1×10^{-7}
C_2H_2		8×10^{-5}			
5-atomic:					
C_5		1×10^{-7}	HC_3N		1×10^{-6}
C_4H		2×10^{-6}	HC_2NC		1×10^{-8}
C_4Si		3×10^{-9}	H_2C_3		2×10^{-9}
c-C_3H_2		2×10^{-8}	SiH_4		2×10^{-7}
CH_4		3×10^{-6}			
6-atomic:					
C_5H		2×10^{-7}	CH_3CN		3×10^{-9}
C_2H_4		2×10^{-8}	H_2C_4		5×10^{-9}
7-atomic:					
C_6H		2×10^{-7}	HC_5N		2×10^{-7}
9-atomic:					
C_8H		3×10^{-9}	HC_7N		4×10^{-8}
11-atomic:					
HC_9N		1×10^{-8}			
Mol. ions:					
HCO^+		1×10^{-9}			

https://doi.org/10.1017/S007418090000961X Published online by Cambridge University Press

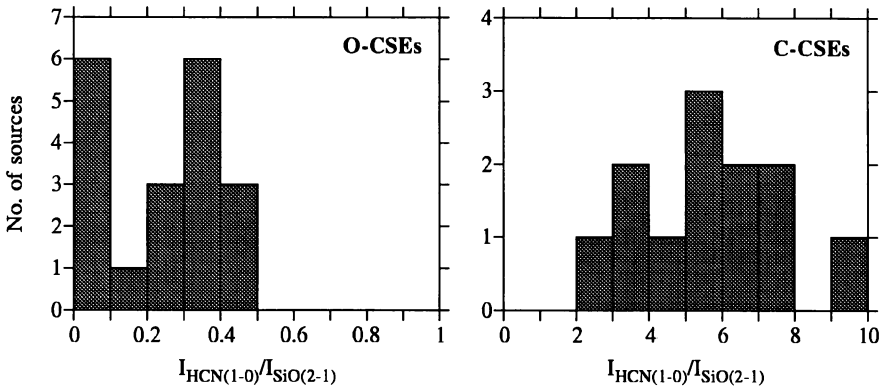

Figure 1. $I_{\mathrm{HCN}(J=1\rightarrow 0)}/I_{\mathrm{SiO}(J=2\rightarrow 1)}$–ratios in AGB O– and C–CSEs (Olofsson et al. 1997).

composition on time scales shorter than the destruction time scale of the molecules, but long enough compared to the available spatial resolution, can also be studied. However, abundance estimates are still uncertain, and the conversion from a circumstellar molecular abundance to the elemental composition is far from trivial, as evidenced for instance by the Cl– and F–compounds in Sect. 4.2.

Observational studies of molecular abundances in objects of different elemental composition have been made by e.g., Lindqvist et al. (1992), Nyman et al. (1993); Olofsson et al. (1993), Omont et al. (1993), Bieging & Latter (1994), Bujarrabal et al. (1994a), and Bachiller et al. (1996). The results are interesting, but they also show the difficulties involved in this problem. We will here only present one simple example in which molecular line intensity ratios are used to distinguish between O– and C–CSEs. The $I_{\mathrm{HCN}(i\rightarrow j)}/I_{\mathrm{SiO}(k\rightarrow l)}$–ratio appears particularly suitable for this task, since HCN is expected to have a low abundance in O–CSEs and a high abundance in C–CSEs, while the opposite should apply to SiO. Indeed, the results in Fig. 1 show that the $I_{\mathrm{HCN}(J=1\rightarrow 0)}/I_{\mathrm{SiO}(J=2\rightarrow 1)}$–ratio strongly discriminates between O– and C–CSEs (see also Bujarrabal et al. 1994b).

6. Isotope ratios

In principle, isotope ratios should be the most reliable since, to first order, the excitation and the spatial distributions should be the same for $\mathrm{X}^{\mathrm{m}}\mathrm{Y}$ and $\mathrm{X}^{\mathrm{n}}\mathrm{Y}$. However, opacity effects, isotope-selective photodissociation, and fractionation may lead to a situation that deviates significantly from the simple relation ${}^{\mathrm{m}}\mathrm{Y}/{}^{\mathrm{n}}\mathrm{Y}=I_{\mathrm{X}^{\mathrm{m}}\mathrm{Y}(u\rightarrow l)}/I_{\mathrm{X}^{\mathrm{n}}\mathrm{Y}(u\rightarrow l)}$. In addition, most of the circumstellar lines are relatively weak, and the observations of the

https://doi.org/10.1017/S007418090000961X Published online by Cambridge University Press

TABLE 3. Isotope ratios in IRC+10216

Isotope ratio	Ratio	IRC/Solar	Species used
$^{12}C/^{13}C$	44	0.5	^{13}CS, $C^{34}S$, $Si^{12}CC$, $Si^{13}CC$
$^{12}C/^{14}C$	>61000		^{13}CO, ^{14}CO
$^{14}N/^{15}N$	5300	20	$H^{13}CN$, $HC^{15}N$
$^{16}O/^{17}O$	840	0.3	^{13}CO, $C^{17}O$
$^{16}O/^{18}O$	1300	3	^{13}CO, $C^{18}O$
$^{28}Si/^{29}Si$	19	1	^{28}SiS, ^{29}SiS, $^{28}SiC_2$, $^{29}SiC_2$
$^{28}Si/^{30}Si$	29	1	^{28}SiS, ^{30}SiS, $^{28}SiC_2$, $^{30}SiC_2$
$^{32}S/^{33}S$	100	1	$Si^{32}S$, $Si^{33}S$
$^{32}S/^{34}S$	20	1	$Si^{32}S$, $Si^{34}S$
$^{35}Cl/^{37}Cl$	2	1	$Na^{35}Cl$, $Na^{37}Cl$, $Al^{35}Cl$, $Al^{37}Cl$
$^{24}Mg/^{25}Mg$	7	1	$^{24}MgNC$, $^{25}MgNC$
$^{24}Mg/^{26}Mg$	7	1	$^{24}MgNC$, $^{26}MgNC$
$^{27}Al/^{26}Al$	>10		$^{27}AlCl$, $^{26}AlCl$, ^{27}AlF, ^{26}AlF

less common isotopic variants become very time consuming.

In this context we will only mention the best studied object so far, IRC+10216. Table 3 summarizes the results for 13 isotope ratios of interest, including upper limits to the radioactive variants ^{26}Al and ^{14}C (see e.g., Cernicharo & Guélin 1987; Kahane et al. 1988, 1992; Guélin et al. 1995; Forestini et al. 1996). This data set can be used together with stellar evolution theories, including mass loss, thermal pulsing, and hot bottom burning, to estimate for instance the main sequence mass of the object (Guélin et al. 1995). Isotope ratio changes with time, $(^{m}Y/^{n}Y)(t)$, are in principle possible to derive from $(I_{X^{m}Y(u\to l)}/I_{X^{n}Y(u\to l)})(r)$.

7. Evolution of the central object

The expansion of the CSE is slow enough, compared to the time scale of the final stellar evolution, that it will provide a common link throughout the transformation from an AGB star to the formation of a PN and a white dwarf. However, the considerable changes in the opacity of the CSE and the intensity and characteristics of the radiation fields, and the occurrence of high–velocity winds and shock formation, result in, often quite drastic, changes in line intensities. It is therefore conceivable that the molecular line pattern of a source can be used to estimate its evolutionary stage.

In Table 4 we list the line intensity ratios $I_{X(u\to l)}/I_{CO(J=1\to 0)}$ for C–CSEs in different evolutionary stages, and the results are also presented in Figure 2 (e.g., Bujarrabal et al. 1988; Bachiller et al. 1989; Cox et al. 1992;

https://doi.org/10.1017/S007418090000961X Published online by Cambridge University Press

TABLE 4. Line intensity ratios, $I_{X(u\to l)}/I_{CO(J=1\to 0)}$, for C–objects

Source	HCN[a]	HNC[a]	HC_3N[b]	SiS[c]	HCO^+[a]	CN[d]	C_2H[d]
AGB–stars:							
IRC+10216	0.71	0.087	0.21	0.11	0.0015	0.89	0.16
CIT6	0.46	0.058	0.12	0.016	0.001	0.78	0.16
CRL3068	0.34	0.14	0.15	0.076		0.24	0.23
pre-PNe:							
CRL2688	0.66	0.054	0.24	0.033	<0.0075	0.39	0.094
CRL618	0.18	0.17	0.12	<0.034	0.13	0.52	0.019
PNe:							
NGC7027	0.13				0.30	0.04	<0.01
M1–16	0.08			<0.02	0.12	0.29	
NGC2346	0.08	0.08			0.064		
NGC6072	0.22	0.049			0.18	0.71	<0.013
IC4406	0.20	0.042			0.16	0.38	<0.015

The [a] $J=1\to 0$, [b] $J=10\to 9$, [c] $J=5\to 4$, [d] $N=1\to 0$ line was used

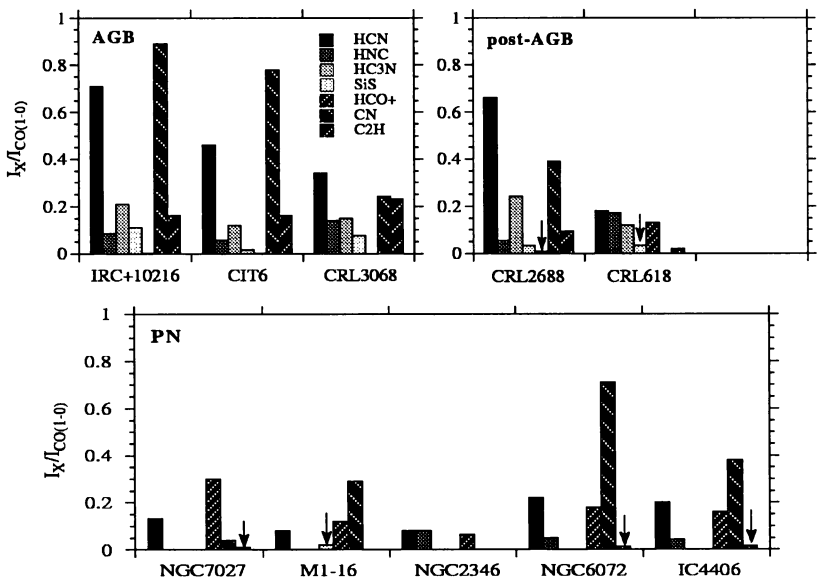

Figure 2. Line intensity ratios, $I_{X(u\to l)}/I_{CO(J=1\to 0)}$, for C–objects in different evolutionary stages (an arrow indicates an upper limit)

Deguchi et al. 1992; Fukasaku et al. 1994; Sahai et al. 1994). The AGB–stars show roughly the same pattern with the HCN and CN lines being the strongest, the other lines are weaker by at least a factor of two, and the

https://doi.org/10.1017/S007418090000961X Published online by Cambridge University Press

HCO^+ line is extremely weak. The young post–AGB object CRL2688 shows essentially the same pattern as the AGB–stars, but for the more evolved object CRL618 the HCN line decreases in strength, while the HCO^+ line gains considerably in strength. In the PNe the HCO^+ line remains strong, and the HCN line and, in particular, the CN line (as opposed to the C_2H line) become strong again. Thus, there appear to be clear trends that can be used to discriminate between objects in different evolutionary stages.

References

Avery L.W., Amano T., Bell M.B., et al. 1992, ApJS 83, 363
Bachiller R., Planesas P., Martín–Pintado J., Bujarrabal V., Tafalla M. 1989, A&A 210, 366
Bachiller R., Fuente A., Bujarrabal V., et al. 1996, A&A, in press
Bakker E.J., van Dishoeck E.F., Waters L.B.F.M., Schoenmaker T. 1996, A&A, in press
Bieging J.H., Latter W.B. 1994, ApJ 422, 765
Bujarrabal V., Gómez-González J., Bachiller R., Martin–Pintado J. 1988, A&A 204, 242
Bujarrabal V., Fuente A., Omont A. 1994a, A&A 285, 247
Bujarrabal V., Fuente A., Omont A. 1994b, ApJ 421, L47
Cernicharo J., Guélin M. 1987, A&A 183, L10
Cernicharo J., Guélin M. 1996, A&A 309, L27
Cox P., Omont A., Huggins P.J., Bachiller R., Forveille T. 1992, A&A 266, 420
Deguchi S., Izumiura H., Nguyen–Q–Rieu, Shibata K.M., Ukita N., Yamamura I. 1992, ApJ 392, 597
Forestini M., Guélin M., Cernicharo J. 1996, A&A, in press
Fukasaku S., Hirahara Y., Masuda A., et al. 1994, ApJ 437, 410
Groesbeck T.D., Phillips T.G., Blake G.A. 1994, ApJS 94, 147
Guélin M., Cernicharo J., Paubert G., Turner B.E., 1990, A&A 230, L9
Guélin M., Lucas R., Cernicharo J. 1993, A&A 280, L19
Guélin M., Forestini M., Valiron P., et al. 1995, A&A 297, 183
Huggins P.J., Olofsson H., Johansson L.E.B. 1988, ApJ 332, 1009
Johnson H.R., Ensman L.M., Alexander D.R., et al. 1995, ApJ 443, 281
Kahane C., Gómez-González J., Cernicharo J., Guélin M. 1988, A&A 190, 167
Kahane C., Cernicharo J., Gómez-González J., Guélin M. 1992, A&A 256, 235
Kastner J. 1992, ApJ 401, 337
Kawaguchi K., Kasai, Y., Ishikawa S., Kaifu N. 1995, PASJ 47, 853
Lindqvist M., Olofsson H., Winnberg A., Nyman L–Å. 1992, A&A 263, 183
Mamon G.A., Glassgold A.E., Huggins P.J. 1988, ApJ 328, 797
Nyman L-Å., Olofsson H., Johansson L.E.B., Booth R.S., Carlström U., Wolstencroft R. 1993, A&A 269, 377
Olofsson H. 1994, in *Circumstellar Media in The Last Stages of Stellar Evolution*, eds R.E.S. Clegg, I.R. Stevens, W.P.S. Meikle (Cambridge University Press, Cambridge), p. 246
Olofsson H. 1997, in *The Carbon Star Phenomenon*, IAU Symposium 177, ed. R. Wing, (Kluwer, Dordrecht), in press
Olofsson H., Eriksson K., Gustafsson B., Carlström U. 1993, ApJS 87, 305
Olofsson H., Bergman P., Eriksson K., Gustafsson B. 1996, A&A 311, 587
Olofsson H., Lindqvist M., Nyman L–Å., Winnberg A. 1997, in prep.
Omont A., Lucas R., Morris M., Guilloteau S. 1993, A&A 267, 490
Sahai R., Wootten A., Schwarz H.E., Wild W. 1994, ApJ 428, 237
Solomon P., Jefferts K.B., Penzias A.A., Wilson R.W. 1971, ApJ 163, L53
Truong–Bach, Morris D., Nguyen–Q–Rieu, Deguchi S. 1990, A&A 230, 431

Turner B.E., Steimle T.C., Meerts L. 1994, ApJ 426, L97
Ziurys L.M., Apponi A.J., Guélin M., Cernicharo J. 1995, ApJ 445, L47

Discussion

Williams: You mentioned that the outflow can cool sufficiently to allow absorption against the cosmic microwave background. Which molecules have been found in absorption?
Olofsson: As far as I am aware of there is one case of a post-AGB object with a very high expansion velocity, where the CO($1 - 0$) line has been detected in absorption, apparently against the cosmic microwave background.

Henning: How good is the assumption that the mass loss rate is constant? New lunar occultation studies show discontinuities in these envelopes.
Olofsson: It is true that the mass loss rate varies both on short ($\leq 10^2$ yrs; perhaps due to the pulsation) and long ($\geq 10^4$ yrs; perhaps due to thermal pulses) time scales. However, the ranges of the emitting regions for most molecular species correspond to a time scale of a few thousand years or less, and the assumption of a constant mass loss rate (when estimating abundances) is therefore probably acceptable for most sources, while on the AGB. Short term variations are averaged out.

Wilson: The $^{18}O/^{17}O$ ratio in the ISM and CSE's is very different from the solar system. Has there been any explanation for this?
Olofsson: The $^{18}O/^{17}O$ ratio of IRC+10216 (≈ 0.7) seems to agree with stellar evolution models for intermediate-mass stars in which ^{17}O should increase and ^{18}O decrease. The higher ratios in the ISM (≈ 3), the Sun (5.5), and starburst galaxies (> 5) could possibly be explained by the larger importance of massive stars.